Grain growth during annealing of cryogenically-rolled Cu-30Zn brass

Tatyana Konkova[1,2], Sergey Mironov[1,3], Alexander Korznikov[1,4], Galia Korznikova[1], Mikhail M. Myshlyaev[5,6], and S.Lee Semiatin[7]

[1] Institute for Metals Superplasticity Problems, Russian Academy of Science, 39 Khalturin Str., Ufa, 450001, Russia

[2] Advanced Forming Research Centre, University of Strathclyde, 85 Inchinnan Drive, Inchinnan, PA4 9LJ United Kingdom

[3] Department of Materials Processing, Graduate School of Engineering, Tohoku University, 6-6-02 Aramaki-aza-Aoba, Sendai 980-8579, Japan [4] National Research Tomsk State University, 36 Lenina av., Tomsk 634050, Russia

[5] Baikov Institute of Metallurgy and Material Science, Russian Academy of Science, 49 Lenin-av., Moscow 119991, Russia

[6] Institute of Solid State Physics, Russian Academy of Sciences, 2 Academic Osypian Str., Chernogolovka, Moscow oblast, 142432, Russia

[7] Air Force Research Laboratory, Materials and Manufacturing Directorate, AFRL/RXCM, Wright-Patterson AFB, OH 45433-7817, USA

The grain-growth behavior of cryogenically-rolled Cue30Zn brass during isothermal annealing at 900 C was examined. The observed microstructure coarsening was interpreted in terms of normal grain growth with a grain-growth exponent of ~4. The relatively slow grain-growth kinetics was attributed to the formation of precipitates at the grain boundaries and the interaction of texture and grain growth. The development of a moderate-strength {110}<uvw> a fiber texture (~4 times random) as well as the presence of a limited number of twin variants within the grains suggested the occurrence of variant selection during annealing.

Keywords: Metal and alloys; Scanning electron microscopy; Metallography; Microstructure; Grain boundaries

1. Introduction

The processing of metals involving large deformation at cryogenic temperatures has recently attracted considerable attention [1-18]. Low deformation temperatures are believed to suppress dynamic recovery and stimulate mechanical twinning, thereby enhancing grain refinement. This may reduce the level of strain necessary to achieve an ultrafine microstructure and thus enable the use of industrial working processes to produce ultrafine-grain materials. The cryogenic deformation is believed to be most effective for the materials prone to mechanical twinning and shear banding, e.g. for Cue30Zn brass [13,14]. In some cases, cryogenic deformation has indeed been reported to be effective in producing substantial grain refinement [2,4,8,10]. For significant commercial application, however, ultrafine-grain materials so

produced must typically be thermally stable over a range of temperatures. Hence, the annealing behavior of cryo-deformed materials is currently of interest.

For pure aluminum and copper, ultrafine-grain structures have been found to be unstable and prone to rapid, discontinuous grain growth [19-22]. Considering the large driving force for grain coarsening in such materials as well as the high density of defects inherent to cryogenic processing, this behavior is not surprising. In cryo-rolled Cu–30Zn brass, on the other hand, only a modicum of microstructure coarsening has been observed at typical recrystallization temperatures, and the ultrafine-grain microstructure has been preserved to ~0.55 T_m (where T_m is the melting point) [23]. The reason for this effect is not completely clear.

The work presented in this article is part of a wide-ranging research program whose goal is to establish the feasibility of applying cryogenic rolling to produce an ultrafine-grain structure in Cu–30Zn brass. The objective of the specific effort reported herein was to quantify the grain-growth behavior of the cryo-rolled material.

2. Material and experimental procedures

The program material comprised Cu–30Zn with a measured composition (in wt. %) of 29.5 Zn, 0.5 Pb, balance Cu, with traces of other elements. The material was produced by ingot casting followed by 10% cold rolling and a subsequent 30 min anneal at 800 C. Sections of this material were then cryogenically rolled to 90-pct. overall thickness reduction (true strain ¼ 2.3) using multiple passes of ~10 pct. each. The final sheet thickness was ~1 mm. In order to provide cryogenic-deformation conditions, the rolling perform and work rolls were soaked in liquid nitrogen prior to each pass and held for 20 min; immediately after each pass, the workpiece was re-inserted into liquid nitrogen. The typical flatrolling convention was adopted in this work; i.e., the rolling, long-transverse, and thickness/normal directions were denoted as RD, TD, and ND, respectively.

To investigate the subsequent grain-growth behavior of the cryo-rolled material, samples were furnace annealed in air at 900 C (0.95 T_m) for times ranging from 1 min to 1 h, followed by water quenching. An additional specimen was quenched immediately upon reaching 900 C.

To provide in-depth insight into the evolution of microstructure and crystallographic texture, characterization was performed using an electron back-scatter diffraction (EBSD) technique. In all cases, the mid-thickness rolling plane (containing the RD and TD) was examined. For this purpose, samples were mechanically ground with water abrasive papers, diamond polished and finally vibratory polished with a colloidal-silica suspension for 24 h. EBSD analysis was conducted using a Hitachi S-4300SE field-emission-gun scanning-electron microscope (FEG-SEM) equipped with a TSL EDAX OIM™ EBSD system. To determine the microstructure at different length scales, several EBSD maps were acquired from each sample using different scan-step sizes ranging from 0.05 to 5 μm. To improve the reliability of the EBSD data, small grains comprising three or fewer pixels were automatically removed from the maps using the grain-dilation

option in the TSL software. Furthermore, to eliminate spurious boundaries caused by orientation noise, a lower-limit boundary-misorientation cutoff of 2was used. A 15 criterion was employed to differentiate low-angle boundaries (LABs) and high-angle boundaries (HABs). Grain size was quantified by the determination of the area of each grain and the calculation of its circle-equivalent diameter.

The chemical composition of different phases in the material was determined using an energy-dispersive X-ray spectroscopy (EDS) system installed in a FEG-SEM Philips XL-30.

3. Results and discussion

3.1. Dezincification

During annealing of Cue30Zn brass at relatively-high temperatures, evaporation of Zn from the free surface (i.e., dezincification) occurred. This effect is well known [24, 25], and was quantified in the present work by determining the concentration of zinc at midthickness rolling plane as a function of annealing time (Fig. 1). It was determined that the zinc content at this location was reduced to ~26 wt. pct. after a 1 h exposure at the annealing temperature.

3.2. Microstructure morphology and grain size

Selected portions of EBSD grain-boundary maps illustrating microstructure evolution during annealing are shown in Fig. 2. In these maps, LABs, HABs, and S3 twin boundaries (within a 5 tolerance) are depicted by red, black, and gray lines, respectively. The corresponding grain-size measurements are summarized in Fig. 3.

The microstructure of the as-cryo-rolled sample (Fig. 2a) was markedly inhomogeneous and could be described in terms of remnants of coarse, original grains with poorly-developed substructure and ultrafine-grain domains. The latter regions consisted of shear bands, mechanical twins, and a dense LAB substructure. The mean grain size of the ultrafine-grain areas was ~0.2 mm. As shown in previous works [13, 14], the formation of this microstructure was related to the very heterogeneous character of deformation twinning during cryogenic rolling.

The cryo-rolled material heated to 900 C, followed immediately by water quenching, revealed a fully-recrystallized grain structure (Fig. 2b). This microstructure was dominated by low-aspect ratio grains containing a significant proportion of annealing twins but almost no LABs. To evaluate the average number of twins per grain, the approach proposed by Field et al. [26] was used. According to this method, the number of grains both including and excluding S3 twin boundaries was measured and quotient of these values was calculated and summarized in Table 1. As follows from the obtained results, the number of twin variants within each recrystallized grain was limited being typically less than three; this presumably indicated the occurrence of variant selection during recrystallization [27]. The grain-size distribution was relatively wide (Fig. 3a) and likely resulted from the specific character of recrystallization of the heterogeneous cryo-rolled microstructure seen in Fig. 2a.

During subsequent soaking at 900 C, the grain structure coarsened substantially (Fig. 3b). In terms of the largest grains, the normalized grain-size distributions became somewhat narrower (Fig. 3a), thus presumably reflecting gradual elimination of the microstructure heterogeneity inherent in the original cryo-rolled state. Nevertheless, the distributions did not change fundamentally with annealing time (Fig. 3a). Together with the similarity of the morphology of the microstructure (Fig. 2bed), these results underlined the relatively continuous character of grain coarsening and an absence of abnormal-like features.

The kinetics of normal grain growth were quantified using the expression

$$D \approx C\tau^{1/n},$$

where D denotes the average grain size, C is constant, t is annealing time, and n is grain-growth exponent [27]. In the ideal case (with grain-boundary energy and mobility independent of misorientation and boundary plane), the grain-growth exponent is typically ~2 [28]. In the present work, however, the exponent was ~4 (Fig. 3c). Several possible sources of this large value of n comprised the nature of the grain boundaries per se, drag associated with solutes or precipitates, and/or the concurrent evolution of crystallographic texture during grain growth. These possibilities are discussed next.

3.3. Nature of the grain boundaries

One possible explanation for the large value of n (and hence slow rate of grain growth) was the character of the grainboundaries. As mentioned in the previous section, the grains typically contained annealing twins and, accordingly, the misorientation distributions were dominated by Σ3 boundaries (Fig. 4).

Additionally, the material also contained some fraction of LABs (Fig. 4a) and their proportion tended to increase with annealing time. Both of these types of boundaries are thought to have low mobility and low energy. In the annealed material, their population constituted ~50 pct. (Fig. 4b) of total grain boundary area and therefore the grain assembly was obviously not ideal. Variable grain-boundary energy is sometimes reported to lead to an increase in the growth exponent n to 4 [27] in agreement with the present results. On the other hand, the value of the exponent has been reported to be 2 in Cue30Zn brass annealed at temperatures between 400 and 700 C, despite extensive annealing twinning [29,30]. Thus, another reason for the present slow grain-growth kinetics was sought.

3.4. Grain-boundary pinning

High-resolution EBSD results revealed that the grain boundaries were not smooth on a local scale, as exemplified in the insert in the top right corner of Fig. 2d. This suggested the possible presence of a pinning agent such as grain-boundary precipitates. High magnification SEM observations (Fig. 5) confirmed this hypothesis. Furthermore, EDS measurements revealed that the precipitate particles were rich in lead; preferential segregation of Sn and P along grain boundaries was also noted by this means. Such grainboundary features could indeed impede grain-boundary motion and result in relatively-slow grain-growth kinetics.

To obtain further insight into this phenomenon, the evolution of the precipitates during annealing was investigated (Figs. 6 and 7). It was determined that the particles precipitated shortly after reaching the annealing temperature (Fig. 6a, b and the higher magnification images in Fig. 7a, b). It was also noted that the precipitates nucleated preferentially at random high-angle boundaries, whereas the annealing-

twin boundaries (of presumably lower interface energy) were typically precipitate-free (Figs. 6b and 7b). These observations suggested perhaps a noticeably different character of diffusion along or in the vicinity of the two types of boundaries.

It was also observed that extensive grain-boundary migration during grain growth produced no significant changes in the character/location of the particles; they remained concentrated primarily at the grain boundaries with almost no precipitates within the interior of the grains (Fig. 6bed). Thus, the particles were likely dragged by the migrating grain boundaries. Such a phenomenon contrasts with solute drag, which is most common at relatively-low homologous temperatures [31], but offers a plausible explanation for the slow grain-growth rate observed herein. Furthermore, the particleeboundary interaction was likely complex and not readily described in terms of the classical Zener-pinning mechanism.

3.5. Texture

To provide additional insight into the observed grain-growth behavior, texture evolution was quantified using the EBSD data. To this purpose, orientation distribution functions (ODFs) were derived from large EBSD maps containing ~1100-23,600 grains (Table 1) and summarized in Fig. 8. For comparative purposes, an ODF indicating the ideal texture components commonly observed in rolled face-centered-cubic metals is shown in Fig. 8a. This ODF can be compared to that for the material in the as-cryo-rolled condition (Fig. 8b) as well as after subsequent annealing at 900 C for various soak times (Fig. 8c-e).

The cryo-rolled material was characterized by a relativelystrong texture which could be described in terms of the superposition of two partial fibers: α<110>//ND and γ<111>//ND; the α- fiber was more pronounced than the γ fiber (Fig. 8b). Within the $_{a}$fiber, strong Brass {110}<112> and Goss {110}<100> components were noted, whereas the γ-fiber was dominated by the Y {111} <112> texture component (Fig. 8b). As shown in previous work [13,14], the Brass and Goss orientations were mainly found in coarse-grain remnants, whereas the γ-fiber and the Y component originated from the ultrafine-grain domains of the cryo-rolled microstructure.

Recrystallization which occurred during heating to the annealing temperature resulted in significant texture changes (Fig. 8c). The recrystallization led to a significant reduction in the sharpness of the texture with the peak intensity decreasing by more than one half. Moreover, the γ-fiber and the Y orientation disappeared almost completely. On the other hand, a new recrystallizationinduced orientation near the Copper (90; 30; 45) component was found (indicated by the arrow in Fig. 8c). This orientation was relatively close to the Brass-R (80; 31; 35) texture component which is often observed during recrystallization of the Cu-30Zn alloy [27].

Remarkably, the recrystallization texture was moderatelystrong (~4.6 times random, Fig. 8c) despite the presence of annealing twins (Fig. 2b). This observation underlies the occurrence of variant selection during twin formation, as noted in Section 3.2.

Soaking at the annealing temperature provided some strengthening of the α-fiber (Fig. 8d-e). The texture sharpening means that grain orientations become somewhat close and thus average misorientation between the grains may decrease. In some cases, the misorientation may even reduce below 15, i.e. high-angle grain

boundary transforms into low-angle boundary. Therefore the strengthening of the α-fiber texture is likely responsible for the observed increase of the fraction of LABs with annealing time (Fig. 4b). Such changes in texture and grain-boundary character are indicative of texture-controlled grain growth for which the gradual development of a strong texture may reduce the average grainboundary energy and mobility. This behavior could thus have provided another factor (in addition to the drag associated with precipitates) that tended to retard the rate of grain growth. In fact, values of n of the order of 4 are not uncommon for such processes, having been observed and modeled (using the Monte-Carlo Potts method) in the past (e.g., [32]).

4. Summary and conclusions

The grain-growth behavior of cryogenically-rolled Cue30Zn brass was investigated. For this purpose, the material was rolled to a 90-pct. thickness reduction at liquid-nitrogen temperature and then isothermally annealed at 900 C (0.95 T_m) for times ranging from 1 min to 1 h; an additional specimen was quenched immediately upon reaching 900 C. Grain-structure and texture changes were followed using an EBSD technique. The main conclusions from this work are as follows.

(1) Due to evaporation of Zn from the material, the concentration of this element was reduced to ~26 wt. pct. after a 1 h anneal.

(2) Despite the strong heterogeneity of the as cryo-rolled microstructure, no evidence of abnormal grain growth was found during annealing. Microstructure evolution can thus be interpreted in terms of recrystallization and annealing twinning followed by normal grain growth.

(3) Recrystallization during heat up to the annealing temperature resulted in a noticeable weakening of the texture developed during cryo-rolling. However, subsequent grain growth during soaking at the annealing temperature promoted some sharpening of {110}<uvw>αfiber orientation. This gave rise to an increase in the fraction of LABs to ~10 pct.

(4) The development of a moderate-strength texture (~4 random) as well as the presence of a limited number of twin variants within grains suggested the occurrence of variant selection during recrystallization.

(5) The grain growth exponent n was measured to be ~4.0; i.e., the grain-growth kinetics were slower than those predicted for a random ensemble of grains whose boundary energy and mobility are isotropic. This observation was attributed to the precipitation of Pb-based particles and segregation of Sn and P along the grain boundaries as well as the possible interaction of texture evolution and grain growth. On the other hand, it is not completely clear whether these two effects were entirely associated with cryogenic deformation per se or may be related with other reasons, e.g. high impurity content or very high annealing temperature. This issue requires additional study.

Acknowledgments

Financial support from the Russian Fund for Fundamental Research (project No.14-02-97004) is gratefully acknowledged. The authors are grateful to P. Klassman for technical assistance in performing the cryogenic-rolling experiments.

References

[1] Y. Estrin, N.V. Isaev, S.V. Lubenets, S.V. Malykhin, A.T. Pugachov, V.V. Pustovalov, E.N. Reshetnyak, V.S. Fomenko, S.E. Shumilin, M. Janecek, R.J. Hellmig, Effect of microstructure on plastic deformation of Cu at low homologous temperatures, Acta Mater. 54 (2006) 5581e5590, http://dx.doi.org/ 10.1016/j.actamat.2006.07.036.

[2] Y.S. Li, N.R. Tao, K. Lu, Microstructural evolution and nanostructure formation in copper during dynamic plastic deformation at cryogenic temperatures, Acta Mater. 56 (2008) 230e241, http://dx.doi.org/10.1016/j.actamat.2007.09.020.

[3] Y. Huang, P.B. Prangnell, The effect of cryogenic temperature and change in deformation mode on the limiting grain size in a severely-deformed dilute aluminum alloy, Acta Mater. 56 (2008) 1619e1632, http://dx.doi.org/10.1016/ j.actamat.2007.12.017.

[4] Y. Zhang, N.R. Tao, K. Lu, Mechanical properties and rolling behaviors of nanograined copper with embedded nano-twin bundles, Acta Mater. 56 (2008) 2429e2440, http://dx.doi.org/10.1016/j.actamat.2008.01.030.

[5] K.P. Sushanta, R. Jayaganathan, A study of the mechanical properties of cryorolled Al-Mg-Si alloy, Mater. Sci. Eng. A 480 (2008) 299e305, http://dx.doi.org/10.1016/j.msea.2007.07.024.

[6] V. Subramanya Sarma, K. Sivaprasad, D. Sturm, M. Heilmaier, Microstructure and mechanical properties of ultra fine grained Cu-Zn and Cu-Al alloys produced by cryorolling and annealing, Mater. Sci. Eng. A 489 (2008) 253e258, http://dx.doi.org/10.1016/j.msea.2007.12.016.

[7] K.P. Sushanta, R. Jayaganathan, V. Chawla, Effect of cryorolling on microstructure of Al-Mg-Si alloy, Mater. Lett. 62 (2008) 2626e2629, http://dx.doi.org/10.1016/j.matlet.2008.01.003.

[8] G.H. Xiao, N.R. Tao, K. Lu, Microstructures and mechanical properties of a CuZn alloy subjected to cryogenic dynamic plastic deformation, Mater. Sci. Eng. A 513e514 (2009) 13e21, http://dx.doi.org/10.1016/j.msea.2009.01.022.

[9] T. Konkova, S. Mironov, A. Korznikov, S.L. Semiatin, Microstructural response of pure copper to cryogenic rolling, Acta Mater. 58 (2010) 5262e5273, http:// dx.doi.org/10.1016/j.actamat.2010.05.056.

[10] J. Das, Evolution of nanostructure in a-brass upon cryorolling, Mater. Sci. Eng. A 530 (2011) 675e679, http://dx.doi.org/10.1016/j.msea.2011.10.002.

[11] S.V. Zherebtsov, G.S. Dyakonov, A.A. Salem, V.I. Sokolenko, G.A. Salishchev, S.L. Semiatin, Formation of nanostructures in commercial-purity titanium via cryorolling, Acta Mater. 61 (2013) 1167e1178, http://dx.doi.org/10.1016/ j.actamat.2012.10.026.

[12] N.K. Kumar, B. Roy, J. Das, Effect of twin spacing, dislocation density, and crystallite size on the strength of nanostructured a-brass, J. Alloys Compd. 618 (2015) 139e145, http://dx.doi.org/10.1016/j.jallcom.2014.08.131.

[13] T. Konkova, S. Mironov, A.V. Korznikov, G. Korznikova, M.M. Myshlyaev, S.L. Semiatin, Grain structure evolution during cryogenic rolling of alpha brass, J. Alloys Compd. 629 (2015) 140e147, http://dx.doi.org/10.1016/ j.jallcom.2014.12.241.

[14] T. Konkova, S. Mironov, A.V. Korznikov, G. Korznikova, M.M. Myshlyaev, S.L. Semiatin, An EBSD investigation of cryogenically-rolled Cu-30%Zn brass, Mater. Character 101 (2015) 173e179, http://dx.doi.org/10.1016/ j.matchar.2015.02.004.

[15] S.K. Panigrahi, R. Jayaganathan, A study on the mechanical properties of cryorolled AleMgeSi alloy, Mater. Sci. Eng. A 480 (2008) 299e305, http://dx.doi.org/10.1016/j.msea.2007.07.024.

[16] S.K. Panigrahi, R. Jayaganathan, V. Chawla, Effect of cryorolling on microstructure of AleMgeSi alloy, Mater. Lett. 62 (2008) 2626e2629, http://dx.doi.org/10.1016/j.matlet.2008.01.003.

[17] V. Subramanya Sarma, J. Wang, W.W. Jian, A. Kauffmann, H. Conrad, J. Freudenberger, Y.T. Zhu, Role of stacking fault energy in strengthening due to cryo-deformation of FCC metals, Mater. Sci. Eng. A 527 (2010) 7624e7630, http://dx.doi.org/10.1016/j.msea.2010.08.015.

[18] K.C. Sekhar, R. Narayanasamy, K. Velmanirajan, Experimental investigations on microstructure and formability of cryorolled AA 5052 sheets, Mater. Des. 53 (2014) 1064e1070, http://dx.doi.org/10.1016/j.matdes.2013.08.008.

[19] G.H. Zahid, Y. Huang, P.B. Prangnell, Microstructure and texture evolution during annealing a cryogenic-SPD processed Al-alloy with a nanoscale lamellar HAGB grain structure, Acta Mater. 57 (2009) 3509e3521, http:// dx.doi.org/10.1016/j.actamat.2009.04.010.

[20] T. Konkova, S. Mironov, A. Korznikov, S.L. Semiatin, Microstructure instability of cryogenically-deformed copper, Scr. Mater. 63 (2010) 921e924, http://dx.doi.org/10.1016/j.scriptamat.2010.07.005.

[21] T. Konkova, S. Mironov, A. Korznikov, S.L. Semiatin, On the room-temperature annealing of cryogenically-rolled copper, Mater. Sci. Eng. A 528 (2011) 7432e7443, http://dx.doi.org/10.1016/j.msea.2011.06.047.

[22] T.N. Konkova, S.Yu Mironov, A.V. Korznikov, M.M. Myshlyaev, S.L. Semiatin, Annealing behaviour of cryogenically-rolled copper, Mater. Sci. Eng. A 585 (2013) 178e189, http://dx.doi.org/10.1016/j.msea.2013.07.042.

[23] T. Konkova, S. Mironov, A.V. Korznikov, G. Korznikova, M.M. Myshlyaev, S.L. Semiatin, Annealing behaviour of cryogenically-rolled Cu-30Zn brass, J. Alloys Comp. 648 (2015) 858e863, http://dx.doi.org/10.1016/ j.jallcom.2015.05.287.

[24] F.W. Giacobbe, Thermodynamic dezincification behavior of brass during annealing, J. Alloys Comp. 202 (1993) 243e250, http://dx.doi.org/10.1016/ 0925-8388(93)90546-Y.

[25] J.-M. Koo, H. Araki, S.-B. Jung, Effect of Zn addition on mechanical properties of brass hollow spheres, Mater. Sci. Eng. A 483e484 (2008) 245e257, http:// dx.doi.org/10.1016/j.msea.2006.01.183.

[26] D.P. Field, L.T. Bradford, M.M. Nowell, T.M. Lillo, The role of annealing twins during recrystallization of Cu, Acta Mater. 55 (2007) 4233e4241, http://dx.doi.org/10.1016/j.actamat.2007.03.021.

[27] F.J. Humphreys, M. Hatherly, Recrystallization and Related Phenomena, Elsevier, 2004, p. 574.

[28] J.E. Burke, D. Turnbull, Recrystallization and grain growth, Prog. Metal. Phys. 3 (1952) 220e292, http://dx.doi.org/10.1016/0502-8205(52)90009-9.

[29] P. Feltham, G.J. Copley, Grain-growth in a-brasses, Acta Metal. 6 (1958) 539e542, http://dx.doi.org/10.1016/0001-6160(58)90170-6.

[30] S.K. Rhee, Grain growth in alpha brass and alpha iron, Mater. Sci. Eng. 9 (1972) 246e248, http://dx.doi.org/10.1016/0025-5416(72)90041-9.

[31] E. Hersent, K. Marthinsen, E. Nes, On the effect of atoms in solid solution on grain growth kinetics, Metall. Mater. Trans. 45A (2014) 4882e4890, http://dx.doi.org/10.1007/s11661-014-2459-y.

[32] O.M. Ivasishin, S.V. Shevchenko, N.L. Vasiliev, S.L. Semiatin, 3D Monte-Carlo simulation of texture-controlled grain growth, Acta Mater. 51 (2003) 1019e1034, http://dx.doi.org/10.1016/S1359-6454(02)00505-0.

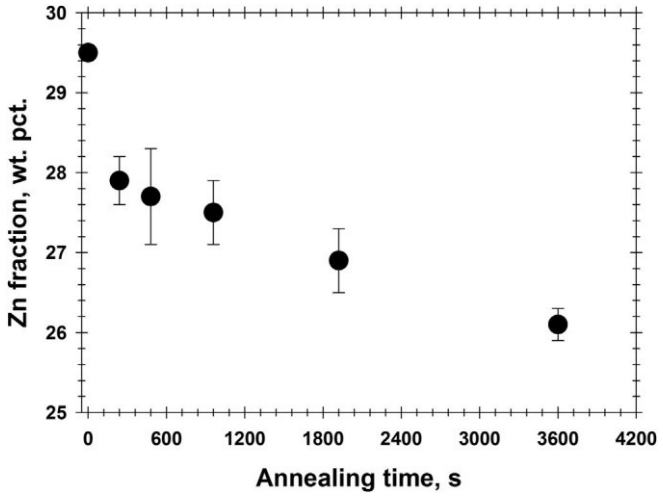

Fig. 1. Effect of annealing time on the evaporation of zinc. Error bars indicate the standard deviation of the measurements.

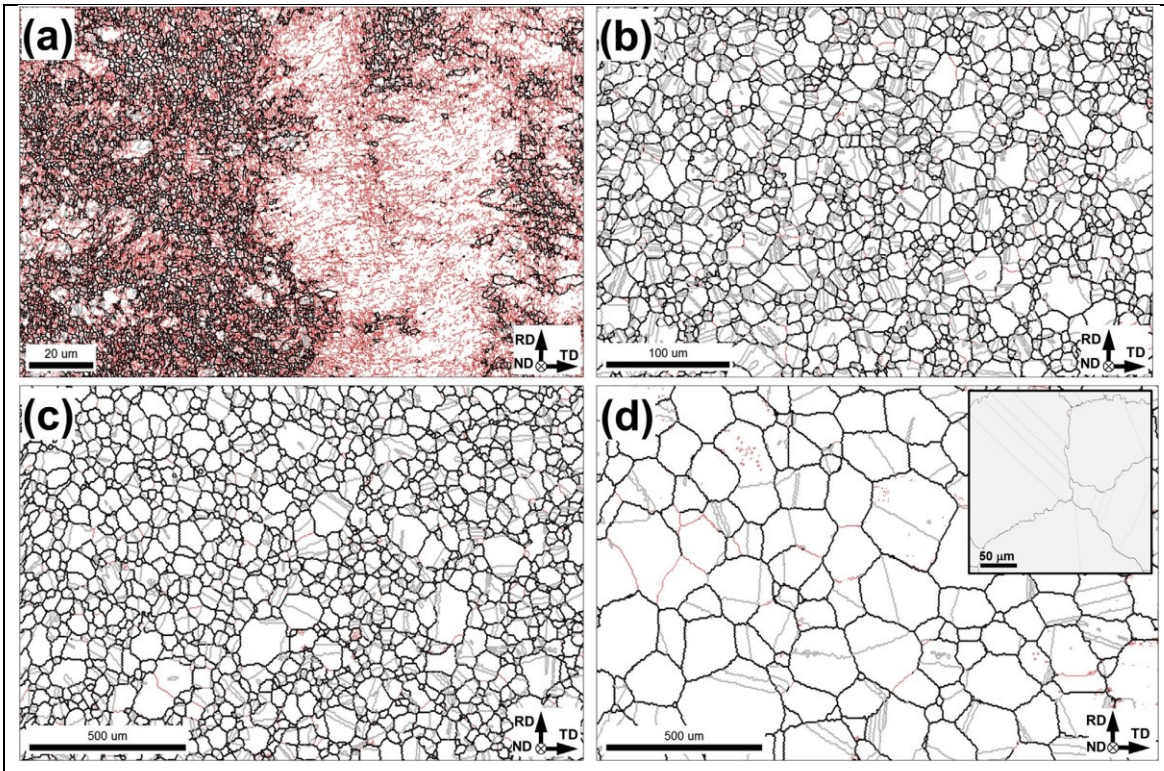

Fig. 2. . Selected portions of grain-boundary EBSD maps showing the grain structure which developed (a) after cryo-rolling and (b) subsequent heating to 900 C and annealing at this temperature for times of (c) 1 min or (d) 1 h. The insert in the top right corner of (d) illustrates the uneven morphology of grain boundaries on a local scale. In the maps, red, black, and gray lines depict LABs, HABs, and Σ3 twin boundaries (within a 5 tolerance), respectively; RD, ND and TD denote the rolling, normal, and transverse directions, respectively. Note the different magnifications. (For interpretation of the references to colour in this figure legend, the reader is referred to the web version of this article

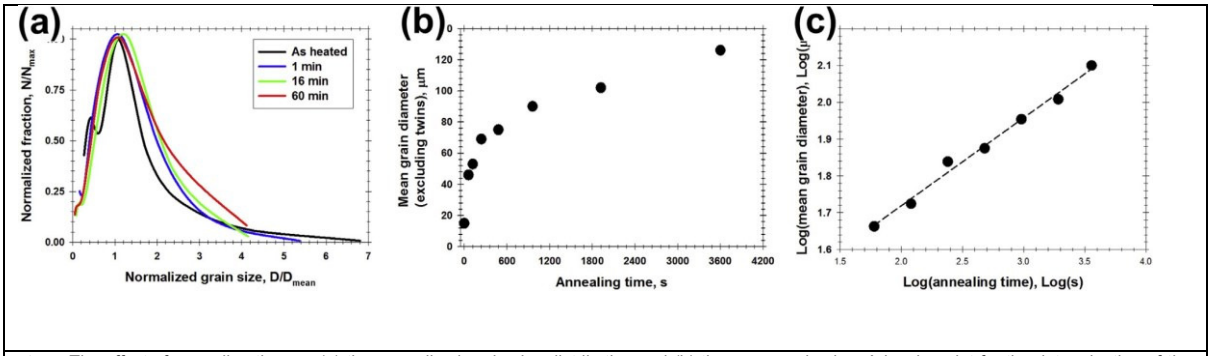

Fig. 3. The effect of annealing time on (a) the normalized grain-size distribution and (b) the mean grain size. A logelog plot for the determination of the grain-growth exponent is shown in (c). In all cases, the grain sizes were measured ignoring annealing-twin boundaries.

Table 1
Measurements of average number of twins per grain.

Material condition	Number of sampled grains		Average number of twins per grain
	Including twins	Excluding twins	
As-cryo-rolled	23,634		
As-heated	17,122	8664	1.976
1 min of annealing	7097	3327	2.105
2 min of annealing	5395	2468	2.186
4 min of annealing	3744	1592	2.352
8 min of annealing	3223	1203	2.679
16 min of annealing	2107	953	2.211
32 min of annealing	1546	688	2.247
60 min of annealing	1109	480	2.310

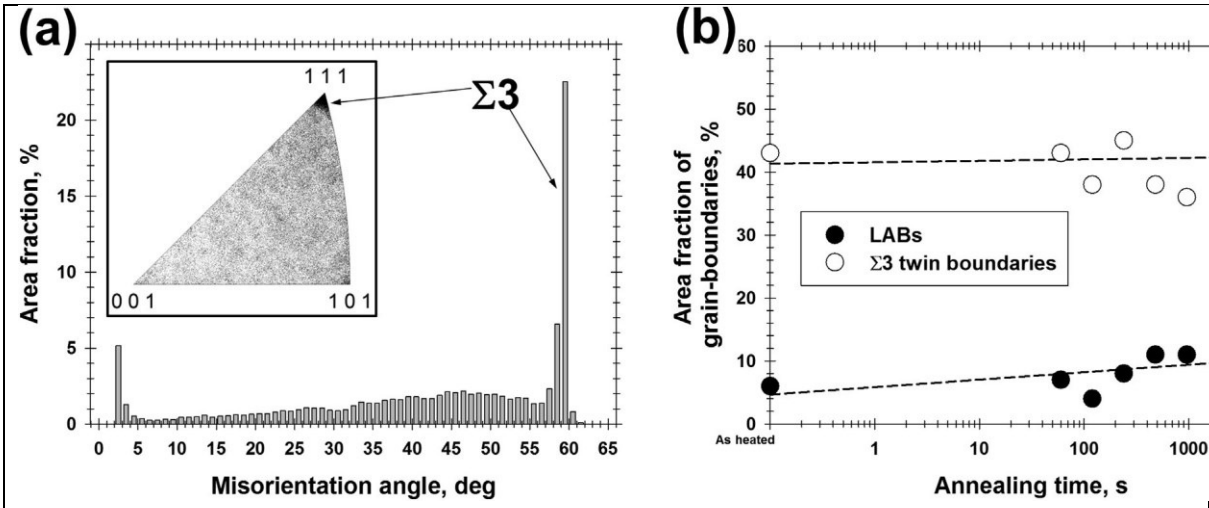

Fig. 4. (a) Typical misorientation distribution and (b) effect of annealing time on the area fraction of LABs and twin boundaries.

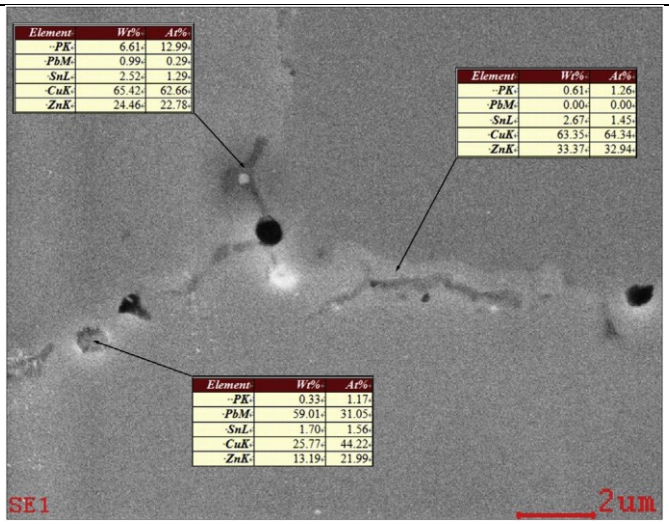

Fig. 5. Measurements of the composition of grain-boundary precipitates.

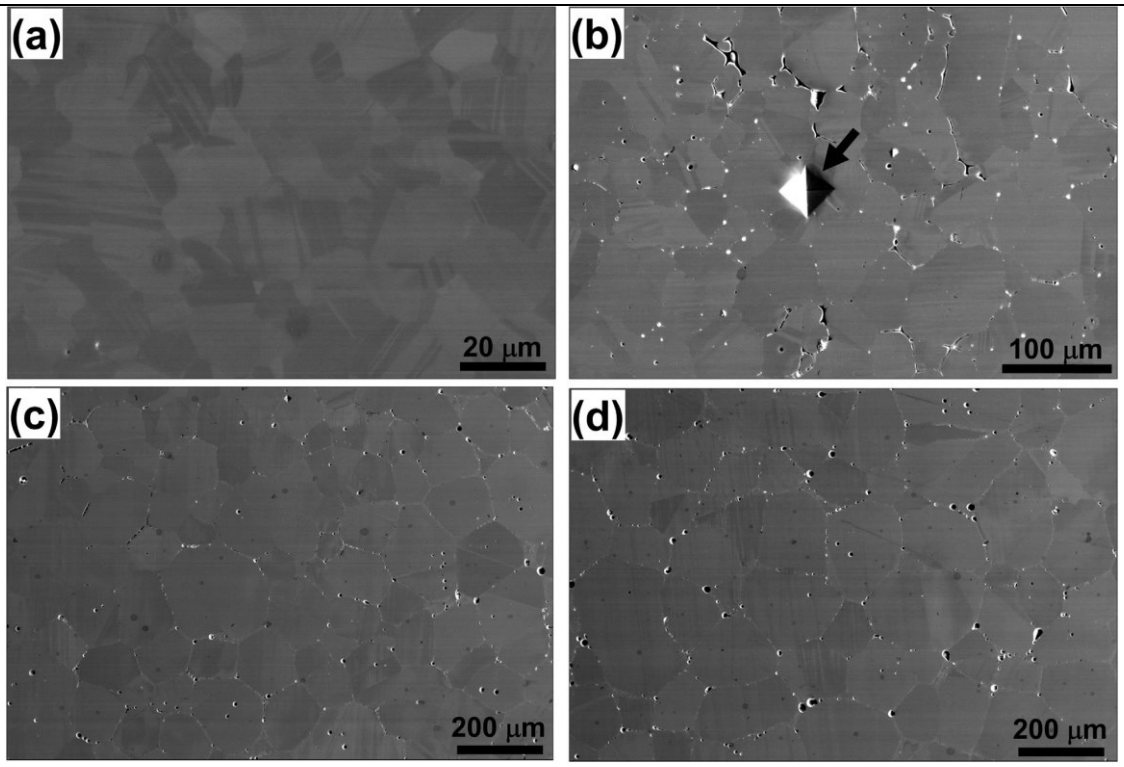

Fig. 6. SEM micrographs illustrating the evolution of Pb-rich particles during annealing: (a) Immediately following heating to 900 C and after subsequent soaking at this temperature for (b) 1 min, (c) 32 min, or (d) 1 h. Note the variation in magnification. The arrow in (b) indicates microhardness indent.

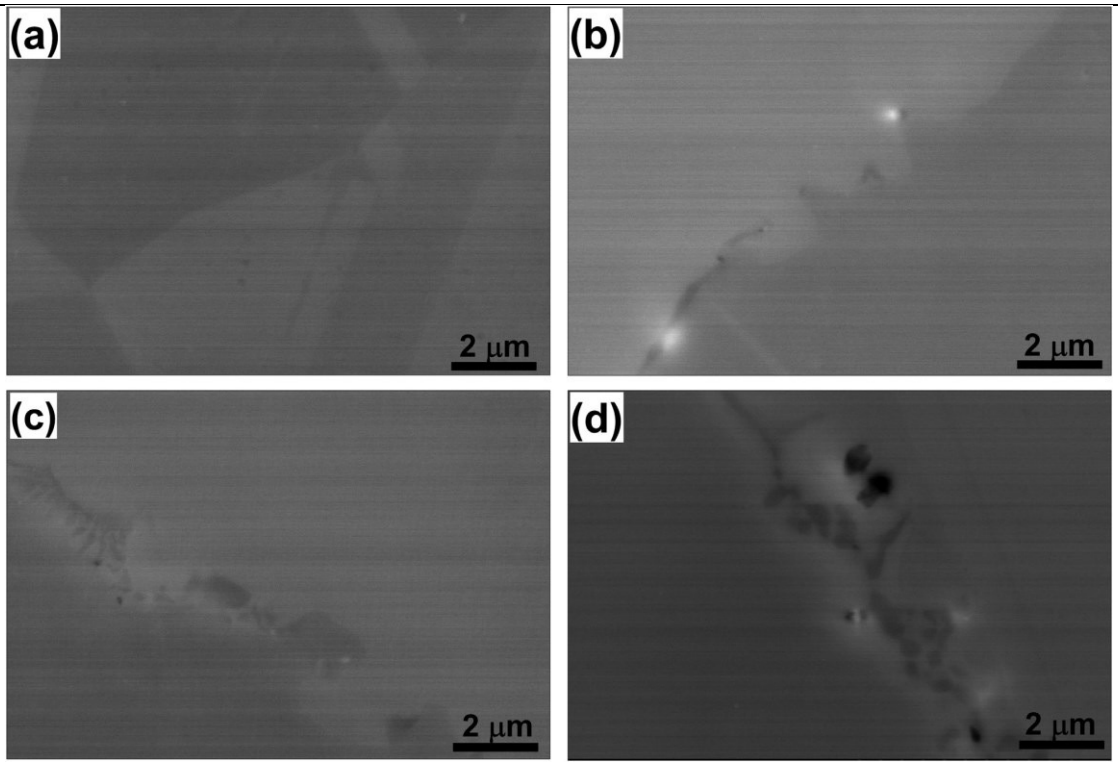

Fig. 7. SEM micrographs illustrating the evolution of P-rich and Sn-rich segregate during annealing: (a) Immediately following heating to 900 C and after subsequent soaking at this temperature for (b) 1 min, (c) 32 min, or (d) 1 h.

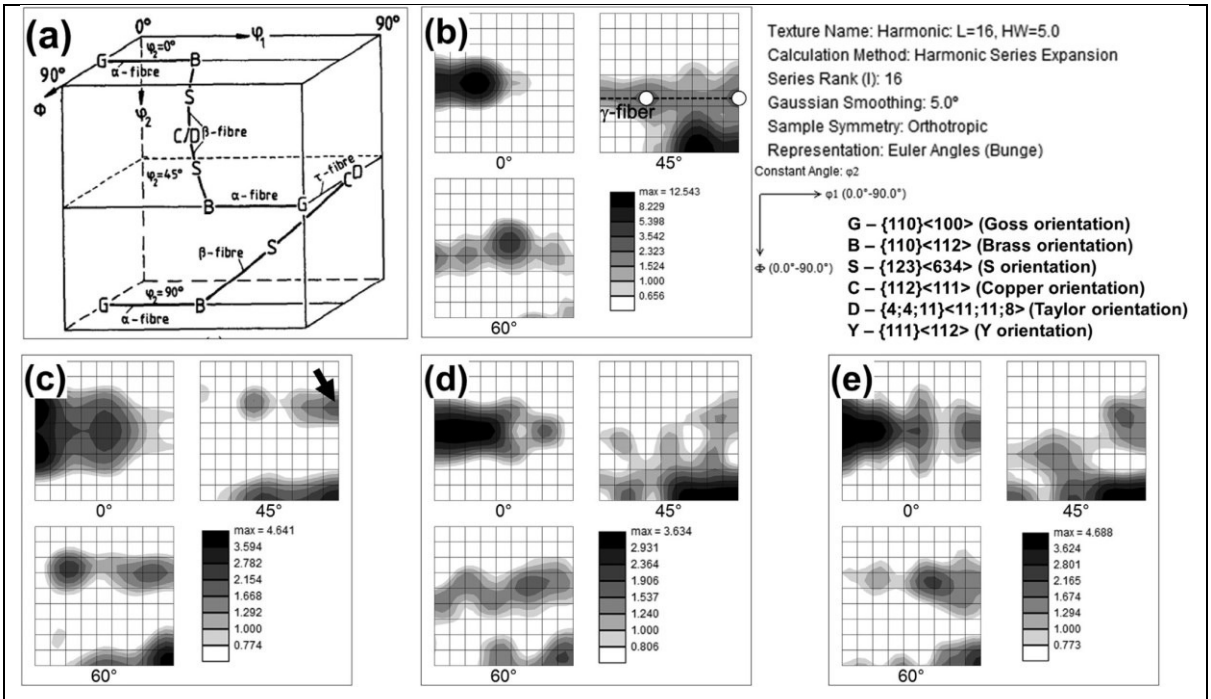

Fig. 8. Orientation distribution functions (ODFs) illustrating (a) ideal rolling texture components for fcc metals, and the textures developed (b) during cryogenic rolling, or cryogenic rolling followed by (c) heating to 900 C and subsequent annealing at this temperature for times of (d) 32 min or (e) 1 h.